Hα SPECTRAL DIVERSITY OF TYPE II SUPERNOVAE: CORRELATIONS WITH PHOTOMETRIC PROPERTIES*

Claudia P. Gutiérrez[1,2], Joseph P. Anderson[2,3], Mario Hamuy[1,2], Santiago González-Gaitán[1,2],
Gastón Folatelli[4], Nidia I. Morrell[5], Maximilian D. Stritzinger[6], Mark M. Phillips[5],
Patrick McCarthy[7], Nicholas B. Suntzeff[8], and Joanna Thomas-Osip[5]
[1] Millennium Institute of Astrophysics, Casilla 36-D, Santiago, Chile
[2] Departamento de Astronomía, Universidad de Chile, Casilla 36-D, Santiago, Chile; cgutierr@das.uchile.cl
[3] European Southern Observatory, Alonso de Córdova 3107, Casilla 19, Santiago, Chile
[4] Institute for the Physics and Mathematics of the Universe (IPMU), University of Tokyo, 5-1-5 Kashiwanoha, Kashiwa, Chiba 277-8583, Japan
[5] Carnegie Observatories, Las Campanas Observatory, Casilla 601, La Serena, Chile
[6] Department of Physics and Astronomy, Aarhus University, Ny Munkegade 120, DK-8000 Aarhus C, Denmark
[7] Observatories of the Carnegie Institution for Science, Pasadena, CA 91101, USA
[8] George P. and Cynthia Woods Mitchell Institute for Fundamental Physics and Astronomy, Department of Physics and Astronomy,
Texas A&M University, College Station, TX 77843, USA

ABSTRACT

We present a spectroscopic analysis of the Hα profiles of hydrogen-rich Type II supernovae. A total of 52 Type II supernovae having well-sampled optical light curves and spectral sequences were analyzed. Concentrating on the Hα P-Cygni profile we measure its velocity from the FWHM of the emission and the ratio of absorption to emission (a/e) at a common epoch at the start of the recombination phase, and search for correlations between these spectral parameters and photometric properties of the V-band light curves. Testing the strength of various correlations we find that a/e appears to be the dominant spectral parameter in terms of describing the diversity in our measured supernova properties. It is found that supernovae with smaller a/e have higher Hα velocities, more rapidly declining light curves from maximum during the plateau and radioactive tail phase, are brighter at maximum light, and have shorter optically thick phase durations. We discuss possible explanations of these results in terms of physical properties of Type II supernovae, speculating that the most likely parameters that influence the morphologies of Hα profiles are the mass and density profile of the hydrogen envelope, together with additional emission components due to circumstellar interaction.

Key word: supernovae: general

Online-only material: color figures

1. INTRODUCTION

Type II Supernovae (SNe II) are produced by the final explosion of massive ($>8\ M_\odot$) stars. They retain a significant part of their hydrogen envelope at the time of the explosion, and hence their spectra show strong Balmer lines. Studies of the variety of SNe II have relied on photometric analysis, cataloging this group into two sub-classes according to the shape of the light curve: SNe with a plateau (quasi-constant luminosity for a period of a few months) are classified as SNe IIP, while SNe with steeper declining linear light curves are classified as SNe IIL (Barbon et al. 1979). However, despite the role played by SNe II in stellar evolution, the impact on their environments, and their importance as standardized candles, an overall picture describing the physics underpinning their diversity is lacking. It has been suggested that SNe IIL are produced by progenitors which explode with smaller mass H envelopes, which then lead to SNe with more linearly declining light curves and shorter or non-existent "plateaus" (Popov 1993). Indeed, this was argued to be the case for the prototype SN IIL 1979C (Branch et al. 1981). This would imply that SNe IIL progenitors suffer from a higher level of mass loss than their IIP counterparts. In addition,

a number of SNe IIL have shown evidence for circumstellar (CSM) interaction at late times (e.g., SN 1986E; Cappellaro et al. 1995; SN 1979C, Milisavljevic et al. 2009), which has been interpreted as evidence of interaction of the ejecta with the pre-supernova CSM (see, e.g., Sahu et al. 2006, Inserra et al. 2013). However, a number of authors have also claimed evidence for signs of CSM interaction in SNe IIP (e.g., SN 1999em, Pooley et al. 2002; SN 2004et, Kotak et al. 2009; SN 2007od, Inserra et al. 2011, Andrews et al. 2010; SN 2009bw, Inserra et al. 2012).

In recent years many individual studies have been published focusing on particular properties of individual SNe, but few statistical studies where the spectral and photometric properties have been directly related are available. Patat et al. (1994) found correlations and anti-correlations between the maximum B-band magnitude (M^B_{max}), the color at maximum (($B - V$)$_{max}$), and the ratio of absorption to emission (e/a) in Hα, concluding that SNe IIL have shallower P-Cygni profiles (larger e/a values) than SNe IIP. Hamuy & Pinto (2002) analyzed 17 SNe IIP and found that SNe with brighter plateaus have higher expansion velocities. Similar results were found by Pastorello et al. (2004) with four SNe II, who concluded that low luminosity SNe have narrow spectral lines indicating low expansion velocities. Hamuy (2003) used observations together with the analytical models of Litvinova & Nadezhin (1983, 1985) to derive physical SN IIP properties. He found that more massive progenitors produce more energetic explosions and in turn produce more nickel. These results were confirmed by Pastorello et al. (2005)

with a heterogeneous group of SNe II that share a very wide range of physical properties.

Despite the above results, it is currently unclear whether underlying spectral and photometric relations exist for the whole ensemble of SN II events. Therefore, here we attempt to remedy this situation by presenting an initial statistical analysis of various spectroscopic and photometric properties of a large sample of SNe II.

In this Letter, we present results showing the diversity of H_α P-Cygni profiles, and relations between spectral and photometric parameters for a sample of 52 SNe. The letter is organized as follows. In Section 2, we outline our SN sample and we define the measurements, then in Section 3 we present the results. In Section 4, possible physical explanations of those results are discussed, and finally in Section 5 we list our conclusions. We note that a detailed analysis of the V-band light curve properties of the currently analyzed sample of SN II is being presented in Anderson et al. (2014, hereafter A14).

2. SN II DATA AND MEASUREMENTS

The sample of SNe II employed in this study was obtained by the Carnegie Supernova Project (CSP; Hamuy et al. 2006) between 2004 and 2009 and by previous campaigns: the Calan/Tololo Supernova Survey (CT), the Cerro Tololo SN program, the Supernova Optical and Infrared Survey (SOIRS), and the Carnegie Type II Supernova Survey (CATS). The full spectroscopic sample will be published in an upcoming paper. Data reductions were performed with IRAF[9] using the standard routines (bias subtracted, flat-field correction, 1D extraction, and wavelength correction). Detailed discussion of spectroscopic observations and reductions for CSP was first presented in Hamuy et al. (2006), then outlined further in Folatelli et al. (2013). These are also applicable to previous data. From this database we selected a subsample of events with sufficient data to measure our spectral and photometric parameters. SN IIn and SN IIb were not analyzed in this work.

SNe II show a large diversity in their spectra. As the dominant spectral feature is the H_α P-cygni profile, for this initial study we concentrate on this line's properties. The H_α line presents a diversity that can be derived from the shape and strength of the emission and absorption, and from the line width. Figure 1 shows the variety in SNe II H_α P-Cygni profiles, where the SNe are ordered in terms of an increasing ratio of absorption to emission (a/e) components (as defined below) around a common epoch at the start of the recombination phase. We see that the absorption is the component which that changes most from one SN to another rather than the emission. There are SNe with little absorption (e.g., SN 2006ai, SN 2006Y), while there are others with boxy absorption profiles (e.g., SN 2003cx, SN 2007X). One can observe in Figure 1 that the first SNe show little absorption compared to emission. The SNe gradually change to show more classic P-Cygni profiles with significant absorption components. A number of SNe show an extra absorption component on the blue side of H_α (e.g., SN 2003hn, SN 2007od, SN 2008aw).

To analyze the SNe spectra within our sample, we define two measurements: (1) the expansion velocity in H_α using the FWHM of the emission, and (2) the ratio of the equivalent
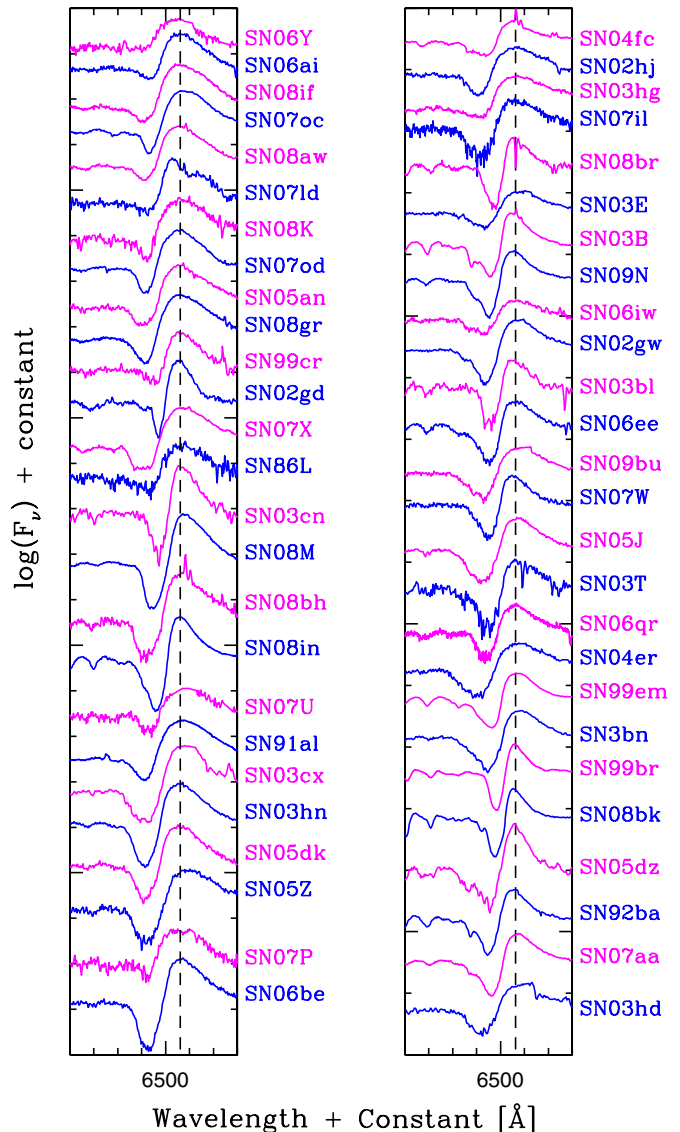

Figure 1. Variety in SN II H_α P-Cygni profiles ordered in terms of increasing a/e starting from the top left panel and ending at the bottom right panel. The host galaxy features were removed and the spectra are shifted to be centered on the peak of the H_α emission. The epochs of the spectra shown are those in closest time proximity to $t_{tran} + 10$. In general, the difference between epochs of the spectra and $t_{tran} + 10$ is within ± 10 days.

(A color version of this figure is available in the online journal.)

widths (EWs) of the absorption to emission (a/e) components of H_α. This ratio was initially proposed by Patat et al. (1994) as the flux ratio of the emission to absorption. However, we choose a/e because in a few SNe, H_α shows an extremely weak absorption component. In order to relate spectral and light curve properties we use the V-band photometric properties as defined by A14: s_1: initial decline from the maximum (magnitudes $100\,d^{-1}$), s_2: "plateau" decline rate (magnitudes $100\,d^{-1}$), s_3: radioactive tail decline (magnitudes $100\,d^{-1}$), M_{max}: magnitude at V-band maximum, and $OPTd$: optically thick phase duration (days): time from the explosion epoch through the end of the plateau phase. We define a common epoch in order to measure spectral properties, which we identified in the light curves: the B-band transition time plus 10 days ($t_{tran} + 10$, at the start of the recombination phase). The transition time is defined as the transition between s_1 and s_2 determined by chi-square minimization. It is measured in the B band because the
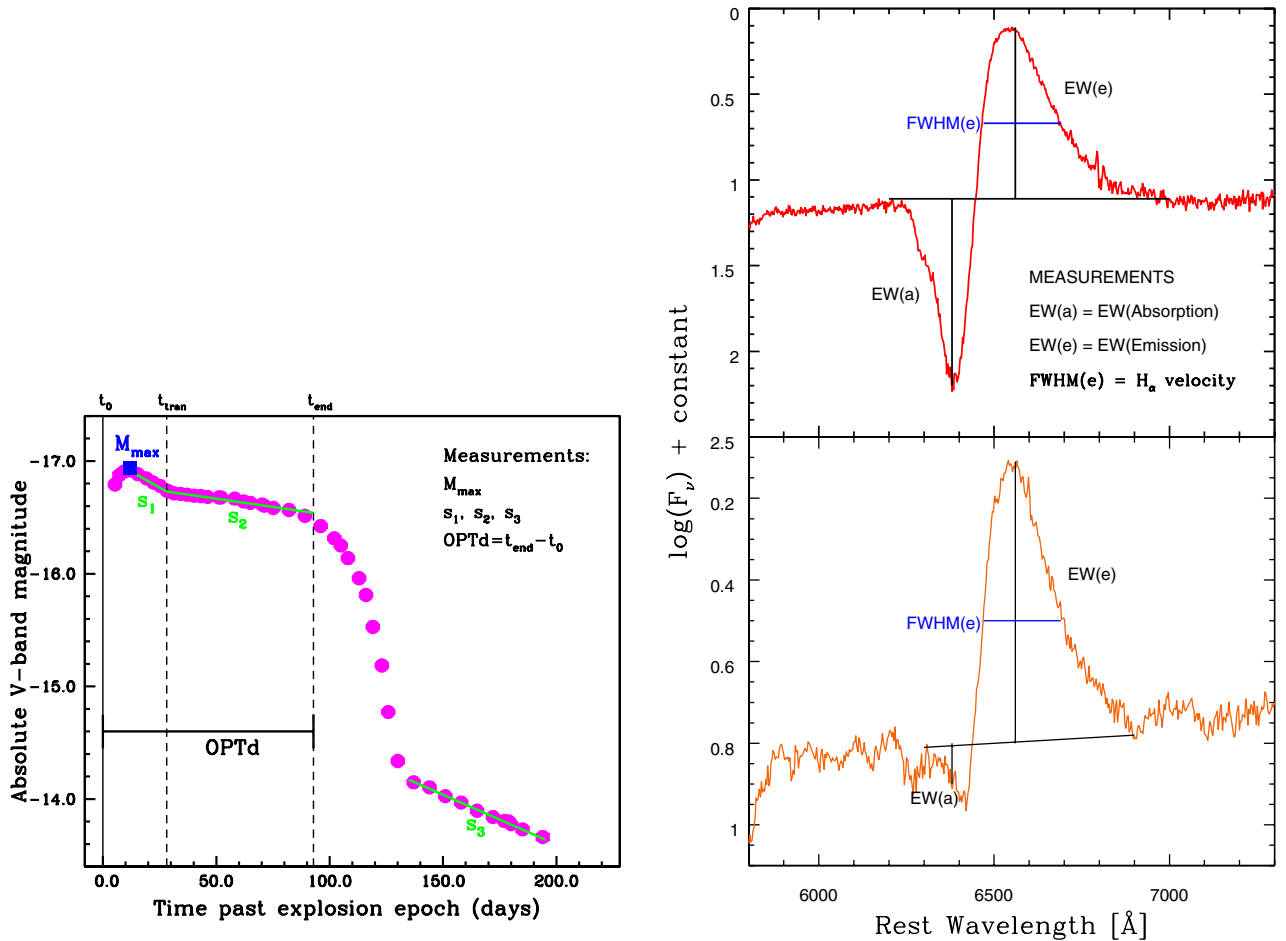
Figure 2. Left: example of the light-curve parameters measured for each SN within the sample in the *V* band (note that while on the figure t_{tran} is shown with respect to *V*-band data, our analysis uses this epoch as defined in the *B* band as this allows us to include more SNe). Observed absolute magnitude at peak, M_{max}, is shown in blue, as applied to the dummy data points (magenta) of an SN IIP. The positions of the three measured slopes, s_1, s_2, and s_3, are shown in green. The optically thick phase duration, *OPTd*, is indicated in black. Three time epochs are labeled: t_0, the explosion epoch; t_{tran}, the transition from s_1 to s_2; and t_{end}, the end of the optically thick phase. Right: examples of spectral measurements. Top: SN 2009bz shows a normal H_α P-Cygni profile with well-defined absorption and emission components. Bottom: SN 2008aw shows a peculiar profile with an extra component on the blue side. In both plots, the blue line represents the FWHM of the emission, which is used for the velocities' values, and the black horizontal line defines the continuum level used to measure the EW of emission and absorption.

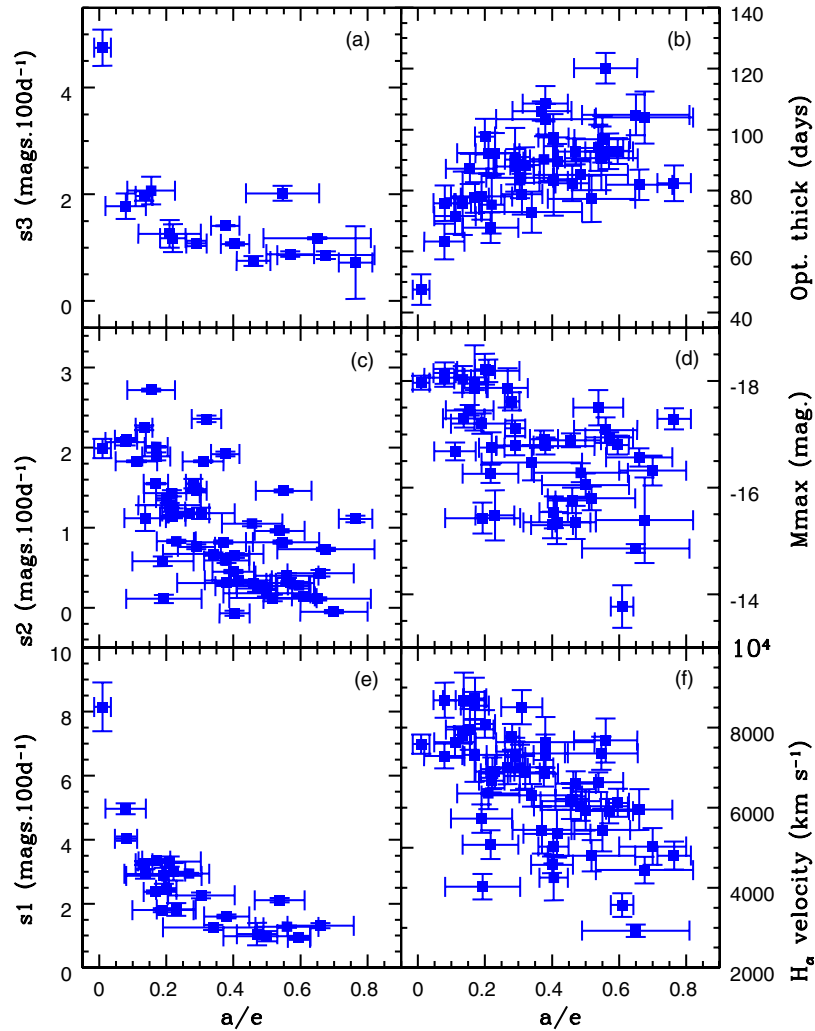(A color version of this figure is available in the online journal.)

transition is more evident than in the *V* band, and therefore we can include more SNe in our analysis. We interpolate all the spectral measurements to this epoch. These parameters are all labeled in the light-curve parameter schematic presented in Figure 2 (left).

To estimate SN ejecta expansion velocities using H_α, the minimum flux of the absorption component of the P-Cygni line profile is commonly used. However, a few SNe in this sample present an extremely weak absorption component, complicating this method. Therefore, we employ the FWHM of the emission line for velocity estimations. To verify the concordance between these methods we measure velocities from the minima of the absorption and the FWHM of the emission in H_α in SNe with a well-defined absorption, finding consistent results. The ratio of absorption to emission (a/e) in H_α was obtained by measuring the EW of each component. Examples of these measurements are shown in Figure 2 (right). The top panel shows a normal H_α P-Cygni profile, i.e., a profile with well defined absorption and emission components, while the bottom panel shows a peculiar profile with an extra absorption component on the blue side. Similar features were identified by Leonard et al. (2001, 2002b, 2002a) in SN 1999em as high velocity (HV) features, while in the case of SN 2005cs the line was identified

as Si II λ6355 absorption (Pastorello et al. 2006). This peculiar structure complicates measurements of the EW of absorption, because it is hard to objectively define the continuum. Therefore, we simply trace a straight line along the absorption feature to mimic the continuum flux, which can be seen in Figure 2 (right). All spectral measurements were performed with IRAF using the *splot* package. The errors for the H_α velocity and a/e are mainly dominated by how the continuum is defined. Errors were obtained by measuring the FWHM and the EW many times, respectively, changing the trace of the continuum. Using these multiple measurements we calculate a mean and take the standard deviation to be the error on that measurement.

3. RESULTS

In Table 1, we list the measured spectral and photometric parameters: H_α velocity, a/e, s_1, s_2, s_3, M_{max}, and *OPTd* for each SN, together with the host galaxy, the heliocentric radial velocity, and t_{tran}. We searched for correlations between all seven of our defined parameters against each other at different epochs: t_{tran}, $t_{tran} - 10$, $t_{tran} + 10$, $t_{tran} + 20$, $t_{tran} + 30$ (measured in the *B* band), and 30 and 50 days since explosion. Using the Pearson correlation test, a/e was observed to be the dominant measured

Figure 3. Relations between a/e, H_α velocity, s_1, s_2, s_3, and M_{max} at $t_{tran} + 10$. Panel A: a/e vs. s_3. Panel B: a/e vs. Optically thick phase. Panel C: a/e vs. s_2. Panel D: a/e vs. M_{max}. Panel E: a/e vs. s_1. Panel F: a/e vs. H_α velocity.

(A color version of this figure is available in the online journal.)

spectral parameter as it has the highest correlation with all other parameters at all epochs. However, at $t_{tran} + 10$ the correlations are strongest, hence this time was chosen as the common epoch. This is justified from a physical point of view because at this epoch all SNe are entering a similar phase in their evolution, i.e., the recombination phase. The photometric parameter s_1 has the highest mean correlation; however, it shows no correlation with the H_α velocity, while s_2 shows high correlation with all parameters. In A14 the photometric correlations are presented. Table 2 shows the strength of the correlations among all our parameters, plus the number of events (within each correlation) and the probability of finding such a correction by chance. The light-curve parameters plus the H_α velocity are plotted versus a/e in Figure 3. The plot shows that SNe with smaller a/e have higher H_α velocities, more rapidly declining light curves after maximum both in the "plateau" and radioactive tail phases, are brighter, and have shorter *OPTd* values. SNe with higher a/e show opposite behavior. Given that *OPTd* and s_3 are most likely related to the envelope/ejecta mass (see A14 for detailed discussion), this would appear to imply that a/e is also related to the mass retained by the progenitor before explosion. Indeed, this further points to SNe being historically classified as IIL (high s_2) as they have smaller mass envelopes at the epoch of explosion than their IIP (low s_2) counterparts. Moreover, we

see a continuum of events in terms of spectral diversity, thus suggesting a possible continuum in pre-SN envelope masses.

In Figure 3, one can see an extreme object, SN 2006Y, specifically in panels A, B, and E. To test whether this object drives our correlations we re-do the Pearson test for all correlations, removing this object. While the strength of the correlations decreases very slightly, all correlations hold, and therefore this object is not driving our results.

We also searched for correlations between a/e and the photospheric velocity, derived from the minimum of absorption of the Fe II $\lambda5169$ Å line at the epoch defined above. However, perhaps surprisingly, no evidence for correlation was found.

4. DISCUSSION

We have presented and analyzed the H_α spectral diversity in 52 SNe II and their correlations with photometric parameters. Analyzing the sample we see a variety in the H_α P-Cygni profiles which can be derived from the shape and strength of the emission and absorption, and from the line width. Patat et al. (1994) found that M_{max}^B and $(B - V)_{max}$ correlate with e/a in H_α, concluding that SNe IIL have larger e/a values (i.e., small a/e values). While in our sample we have not made distinctive IIP–IIL classification, our results are consistent with those of

Table 1
SNe II Spectral and Photometric Parameters

SN	Host Galaxy	Recession Velocity (km s^{-1})	t_{tran} (MJD)	M_{max} (mag)	s_1 (mag 100 d^{-1})	s_2 (mag 100 d^{-1})	s_3 (mag 100 d^{-1})	$Optd$ (days)	a/e	H_α Velocity (km s^{-1})
1986L	NGC 1559	1305	46747.4 ± 0.5	−18.19 ± 0.2	3.32 ± 0.16	1.28 ± 0.03	⋯	92.24 ± 6.71	0.21 ± 0.09	6354 ± 392
1991al	LEDA 140858	4575	48478.1 ± 1.3	−17.62 ± 0.2	⋯	1.55 ± 0.06	1.26 ± 0.26	⋯	0.28 ± 0.02	7771 ± 320
1992ba	NGC 2082	1185	48926.3 ± 1.0	−15.39 ± 0.8	⋯	0.73 ± 0.02	0.86 ± 0.07	103.97 ± 8.54	0.68 ± 0.14	4439 ± 334
1999br	NGC 4900	960	51308.4 ± 0.5	−13.77 ± 0.4	⋯	0.14 ± 0.02	⋯	⋯	0.61 ± 0.03	3566 ± 297
1999cr	ESO 576-G034	6 069	51273.6 ± 0.7	−17.20 ± 0.2	1.80 ± 0.06	0.58 ± 0.06	⋯	78.06 ± 7.62	0.19 ± 0.09	5728 ± 357
1999em	NGC 1637	717	51509.7 ± 0.7	−16.94 ± 0.1	⋯	0.31 ± 0.02	0.88 ± 0.05	92.86 ± 5.83	0.57 ± 0.07	5915 ± 306
2002gd	NGC 7537	2676	52581.6 ± 0.8	−15.43 ± 0.3	2.87 ± 0.25	0.11 ± 0.05	⋯	⋯	0.19 ± 0.11	4023 ± 320
2002gw	NGC 922	3084	52583.1 ± 1.0	−15.76 ± 0.2	⋯	0.30 ± 0.03	0.75 ± 0.09	82.33 ± 5.83	0.46 ± 0.05	6217 ± 274
2002hj	NPM1G +04.0097	7080	52595.8 ± 3.1	−16.91 ± 0.2	⋯	1.92 ± 0.03	1.41 ± 0.01	90.24 ± 7.62	0.38 ± 0.04	6857 ± 334
2003B	NGC 1097	1272	52666.2 ± 1.9	−15.54 ± 0.3	⋯	0.65 ± 0.03	1.07 ± 0.03	83.19 ± 11.4	0.40 ± 0.04	4251 ± 658
2003E	MCG -4-12-004	4470	52661.5 ± 3.5	⋯	⋯	−0.07 ± 0.03	⋯	97.42 ± 7.62	0.40 ± 0.04	5028 ± 424
2003T	UGC 4864	8373	52686.8 ± 1.5	⋯	⋯	0.82 ± 0.02	2.02 ± 0.14	90.59 ± 10.44	0.55 ± 0.11	7360 ± 411
2003bl	NGC 5374	4377	52736.7 ± 1.2	−15.35 ± 0.3	1.05 ± 0.35	0.24 ± 0.04	⋯	92.81 ± 4.24	0.47 ± 0.06	6596 ± 311
2003bn	2MASX J10023529	3831	52729.7 ± 8.6	−16.80 ± 0.2	0.93 ± 0.06	0.28 ± 0.04	⋯	92.97 ± 4.24	0.60 ± 0.03	6121 ± 352
2003cn	IC 849	5433	52743.6 ± 1.7	−16.26 ± 0.2	⋯	1.43 ± 0.04	⋯	67.80 ± 5.00	0.22 ± 0.08	5074 ± 361
2003cx	NEAT J135706.53	11100	52754.7 ± 4.2	−16.79 ± 0.2	⋯	0.76 ± 0.03	⋯	87.82 ± 5.83	0.29 ± 0.05	7314 ± 343
2003hd	MCG -04-05-010	11850	52886.9 ± 1.6	−17.29 ± 0.2	⋯	1.11 ± 0.04	0.72 ± 0.68	82.39 ± 5.83	0.76 ± 0.05	4800 ± 350
2003hg	NGC 7771	4281	52898.3 ± 3.3	⋯	1.60 ± 0.06	0.59 ± 0.03	⋯	108.50 ± 5.83	0.38 ± 0.07	7360 ± 466
2003hn	NGC 1448	1170	52900.9 ± 3.9	−17.11 ± 0.1	⋯	1.46 ± 0.02	1.08 ± 0.05	90.10 ± 10.44	0.29 ± 0.03	7268 ± 375
2004er	MCG -01-7-24	4411	53319.3 ± 0.4	−17.08 ± 0.2	1.28 ± 0.03	0.40 ± 0.03	⋯	120.15 ± 5.00	0.56 ± 0.09	7680 ± 553
2004fc	NGC 701	1831	53335.7 ± 0.4	⋯	⋯	0.82 ± 0.02	⋯	106.06 ± 3.16	0.37 ± 0.09	5440 ± 585
2005an	SO 506-G11	3206	53466.1 ± 0.3	⋯	3.34 ± 0.06	1.89 ± 0.05	⋯	77.71 ± 5.00	0.17 ± 0.04	8548 ± 343
2005dk	C 4882	4708	53638.4 ± 0.9	⋯	2.26 ± 0.09	1.18 ± 0.07	⋯	84.22 ± 6.71	0.30 ± 0.10	7008 ± 567
2005dz	GC 12717	5696	53666.7 ± 0.8	−16.57 ± 0.2	1.31 ± 0.08	0.43 ± 0.04	⋯	81.86 ± 5.00	0.66 ± 0.10	5952 ± 512
2005J	NGC 4012	4183	53421.1 ± 0.4	−17.50 ± 0.3	2.11 ± 0.07	0.96 ± 0.02	⋯	94.03 ± 7.62	0.54 ± 0.07	6637 ± 245
2005Z	NGC 3363	5766	53432.9 ± 1.0	⋯	⋯	1.83 ± 0.01	⋯	78.84 ± 6.71	0.31 ± 0.06	8512 ± 430
2006Y	anon	10074	53794.7 ± 0.6	−17.97 ± 0.13	8.15 ± 0.76	1.99 ± 0.12	4.75 ± 0.34	47.49 ± 5.00	0.01 ± 0.02	7588 ± 244
2006ai	ESO 005- G 009	4571	53813.7 ± 1.0	−18.06 ± 0.2	4.97 ± 0.17	2.07 ± 0.04	1.78 ± 0.24	63.26 ± 5.83	0.08 ± 0.06	7291 ± 307

Table 1
(Continued)

SN	Host Galaxy	Recession Velocity (km s^{-1})	t_{tran} (MJD)	M_{max} (mag)	s_1 (mag 100 d^{-1})	s_2 (mag 100 d^{-1})	s_3 (mag 100 d^{-1})	$Optd$ (days)	a/e	H_α Velocity (km s^{-1})
2006be	IC 4582	2145	53835.4 ± 0.5	−16.47 ± 0.3	1.26 ± 0.08	0.67 ± 0.02	· · ·	72.89 ± 6.71	0.34 ± 0.15	6308 ± 283
2006ee	NGC 774	4620	53997.2 ± 1.3	−16.28 ± 0.2	· · ·	0.27 ± 0.02	· · ·	85.17 ± 5.00	0.49 ± 0.14	6034 ± 366
2006iw	2MASX J23211915	9226	54049.40 ± 1.9	−16.89 ± 0.1	· · ·	1.05 ± 0.03	· · ·	· · ·	0.46 ± 0.09	6162 ± 448
2006qr	MCG -02-22-023	4350	54098.2 ± 1.2	· · ·	· · ·	1.46 ± 0.02	· · ·	96.85 ± 7.62	0.55 ± 0.08	5440 ± 535
2007aa	NGC 4030	1465	54162.7 ± 0.8	−16.32 ± 0.3	· · ·	−0.05 ± 0.02	· · ·	· · ·	0.70 ± 0.10	5028 ± 462
2007il	IC 1704	6454	54393.4 ± 2.0	−16.78 ± 0.2	· · ·	0.31 ± 0.02	· · ·	103.43 ± 5	0.38 ± 0.15	7634 ± 636
2007ld	SDSS J204929.40	8994	54402 ± 1.9	−17.30 ± 0.2	2.93 ± 0.15	1.12 ± 0.16	· · ·	· · ·	0.14 ± 0.06	8685 ± 690
2007oc	NGC 7418	1450	54419.8 ± 0.4	−16.68 ± 0.2	· · ·	1.83 ± 0.01	· · ·	71.62 ± 5.83	0.11 ± 0.06	7634 ± 386
2007od	UGC 12846	1734	54427.7 ± 0.3	−17.87 ± 0.8	2.37 ± 0.05	1.55 ± 0.01	· · ·	· · ·	0.17 ± 0.04	7314 ± 672
2007P	ESO 566-G36	12224	54154.9 ± 3.2	· · ·	· · ·	2.36 ± 0.04	· · ·	88.33 ± 5.83	0.32 ± 0.04	6880 ± 410
2007U	ESO 552-65	7791	54168.8 ± 1.7	−17.87 ± 0.4	2.94 ± 0.02	1.18 ± 0.01	· · ·	· · ·	0.27 ± 0.06	6994 ± 407
2007W	NGC 5105	2902	54164.3 ± 1.0	−15.80 ± 0.2	· · ·	0.12 ± 0.04	· · ·	77.29 ± 7.62	0.52 ± 0.13	4800 ± 392
2007X	ESO 385-G32	2837	54180.8 ± 0.3	−18.22 ± 0.3	2.43 ± 0.06	1.37 ± 0.03	· · ·	97.71 ± 5.83	0.20 ± 0.03	8091 ± 346
2008aw	NGC 4939	3110	54563.8 ± 0.6	−18.03 ± 0.2	3.27 ± 0.06	2.25 ± 0.03	1.97 ± 0.09	75.83 ± 10.44	0.13 ± 0.02	7817 ± 398
2008bh	NGC 2642	4345	54593.0 ± 2.6	· · ·	3.00 ± 0.27	1.20 ± 0.04	· · ·	· · ·	0.22 ± 0.03	6857 ± 397
2008bk	NGC 7793	227.	54602.3 ± 1.4	−14.86 ± 0.1	· · ·	0.11 ± 0.02	1.18 ± 0.02	104.83 ± 6.71	0.65 ± 0.16	2925 ± 155
2008br	IC 2522	3019	54579.2 ± 1.6	−15.30 ± 0.2	· · ·	0.45 ± 0.02	· · ·	· · ·	0.40 ± 0.06	4571 ± 205
2008gr	IC 1579	6831	54801.8 ± 0.9	−17.95 ± 0.1	· · ·	2.01 ± 0.01	· · ·	· · ·	0.17 ± 0.03	8731 ± 521
2008if	MCG -01-24-10	3440	54850.0 ± 0.4	−18.15 ± 0.2	4.03 ± 0.07	2.10 ± 0.02	· · ·	75.85 ± 5.83	0.08 ± 0.03	8685 ± 441
2008in	NGC 4303	1566	54851.5 ± 0.8	−15.48 ± 0.5	1.82 ± 0.20	0.83 ± 0.02	· · ·	92.20 ± 6.71	0.23 ± 0.06	6903 ± 416
2008K	ESO 504-G5	7997	54513.0 ± 1.2	−17.45 ± 0.1	· · ·	2.72 ± 0.02	2.07 ± 0.26	87.11 ± 5.00	0.16 ± 0.07	7954 ± 511
2008M	ESO 121-26	2267	54508.9 ± 0.6	−16.75 ± 0.3	· · ·	1.14 ± 0.02	1.18 ± 0.26	75.34 ± 9.49	0.22 ± 0.04	6674 ± 290
2009bu	NGC 7408	3494	54940.1 ± 1.0	−16.05 ± 0.2	0.98 ± 0.16	0.18 ± 0.04	· · ·	· · ·	0.50 ± 0.13	5943 ± 516
2009N	NGC 4487	1034	54877.1 ± 0.5	−15.35 ± 0.4	· · ·	0.34 ± 0.01	· · ·	89.50 ± 5.83	0.41 ± 0.10	5348 ± 599

Notes. Measurements made of our sample of SNe as mentioned in Section 2. The first three columns present the SNe name and the host galaxy information: host galaxy name and their recession velocities. From Columns 4 to 9 the photometric measurements: t_{tran} (in B-band), M_{max}, s_1, s_2, s_3, and $Optd$ (in V band) are presented. In Column 10, we present the a/e, followed by the H_α velocity.

Table 2
Pearson's r-parameter Which Indicates the Strength of the Correlation, Together with the Number of Events in Parentheses, and the Probability of Finding Such Correlation by Chance

$\cdots$	a/e	H_α Vel.	s_1	s_2	s_3	M_{max}	Opt. Thick
a/e	$\cdots$	$-0.60\ (52;\ 2.05\times10^{-6})$	$-0.74\ (23;\ 4.63\times10^{-5})$	$-0.65\ (52;\ 1.63\times10^{-7})$	$-0.64\ (15;\ 0.01)$	$-0.53\ (42;\ 2.82\times10^{-4})$	$0.56\ (40;\ 1.90\times10^{-4})$
H_α vel.	$-0.60\ (52;\ 2.05\times10^{-6})$	$\cdots$	$0.34\ (23;\ 0.11)$	$0.64\ (52;\ 2.39\times10^{-7})$	$0.51\ (15;\ 0.05)$	$-0.77\ (42;\ 2.83\times10^{-9})$	$-0.19\ (40;\ 0.23)$
s_1	$-0.74\ (23;\ 4.63\times10^{-5})$	$0.34\ (23;\ 0.11)$	$\cdots$	$0.74\ (23;\ 5.02\times10^{-5})$	$0.94\ (4;\ 0.06)$	$0.54\ (19;\ 0.02)$	$-0.73\ (17;\ 8.10\times10^{-4})$
s_2	$-0.65\ (52;\ 1.63\times10^{-7})$	$0.64\ (52;\ 2.39\times10^{-7})$	$0.74\ (23;\ 5.02\times10^{-5})$	$\cdots$	$0.54\ (15;\ 0.40)$	$0.70\ (42;\ 2.02\times10^{-7})$	$-0.46\ (40;\ 2.80\times10^{-3})$
s_3	$-0.64\ (15;\ 0.01)$	$0.51\ (15;\ 0.05)$	$0.94\ (4;\ 0.06)$	$0.54\ (15;\ 0.40)$	$\cdots$	$0.48\ (14;\ 0.08)$	$-0.72\ (15;\ 2.60\times10^{-3})$
M_{max}	$-0.53\ (42;\ 2.82\times10^{-4})$	$0.77\ (42;\ 2.83\times10^{-9})$	$0.54\ (19;\ 0.02)$	$0.70\ (42;\ 2.02\times10^{-7})$	$0.48\ (14;\ 0.08)$	$\cdots$	$-0.28\ (31;\ 0.12)$
$OPTd$	$0.56\ (40;\ 1.90\times10^{-4})$	$-0.19\ (40;\ 0.23)$	$-0.73\ (17;\ 8.10\times10^{-4})$	$-0.46\ (40;\ 2.80\times10^{-3})$	$-0.72\ (15;\ 2.60\times10^{-3})$	$-0.28\ (31;\ 0.12)$	$\cdots$

Patat et al. (1994), which show that SNe with high s_2 values (faster declining light curves) have small a/e values and are more luminous.

Arcavi et al. (2012) identified a subdivision of SNe II (based on 21 events in the R band), suggesting that SNe IIL and SNe IIP are not members of one continuous class and may result from different physical progenitor systems. However, A14, with a bigger sample (116 events in the V band), suggest an observational continuum of events which may be driven by differences in envelope mass at the epoch of explosion, a parameter which is most directly constrained in A14 through observations of the optically thick phase duration (*OPTd*) and the decline rate during the radioactive tail (s_3). This conclusion of an observational continuum is also supported by the spectral analysis presented in this paper (see Figure 3), where differences in the spectral parameters (especially a/e) may also be explained by changes in the hydrogen envelope mass retained.

Schlegel (1996) discussed possible explanations for the behavior of the H_α P-Cygni profile with the most likely being: (1) extra emission fills in the absorption component (as can be seen in SN 2008aw, Figure 2, bottom); (2) the envelope mass is low; and (3) a steep density gradient in the hydrogen envelope. The first explanation invokes emission scattering off either CSM or the outer envelope (in the case of very extended envelope). The second explanation is described in a low-mass envelope, where there is less absorbing material, so little P-Cygni absorption component will be formed. The third explanation argues that a very steep density gradient implies less absorbing material at high velocities, and so does not produce a well-defined P-Cygni profile. Although these considerations could explain the diversity found in our sample, numerous studies discuss other explanations based on the complex P-Cygni line profiles. Baron et al. (2000) created the term "complicated P-Cygni profile" to explain the double P-Cygni absorption found in Balmer Series and He I λ5876 in SN 1999em, concluding that these absorption features arise in two velocity regions in the expanding ejecta of the SN at different velocities. Pooley et al. (2002) argue that this extra component might be the signature of weak interaction with a low density CSM, while Chugai et al. (2007) attributes these features to ejecta wind interactions. In conclusion, the change in the H_α P-Cygni profile (a/e and FWHM of emission) is most likely related to two parameters: changes in the envelope properties (i.e., its mass and density profile) and the degree of CSM interaction. Although the possible explanations for the behavior of the H_α P-Cygni profile have been exposed, these extra components could be attributed to HV H I features or absorption lines of other ions (Si II). This issue will be further explored after a full spectral analysis. This will determine if similar features are also present in the blue side of the He I λ5876 and H_β.

5. CONCLUSIONS

We presented an initial analysis of the spectral diversity H_α of SNe II and how this relates to light-curve properties. We found that while much diversity and peculiarities exist, spectral and photometric properties do appear to be correlated, which can be linked to pre-SN properties. Our main conclusions are as follows.

1. a/e is an important parameter describing the spectral diversity of SNe II.
2. SNe with low a/e values appear to have high H_α velocities and decline rates, are brighter, and have a smaller *OPTd* values.

3. While any definitive spectral distinction between IIP and IIL is not clear, SNe with higher s_2 values (i.e., more "linear" SNe) have smaller a/e values, have higher H_α velocities, and are more luminous.
4. We speculate that the envelope mass retained before explosion and the density gradient play a very important role to determine the differences of H_α P-Cygni profile.
5. CSM interaction could also be a cause of the change in the P-Cygni profiles, suggesting that faster declining SNe have more intense interactions.

This Letter presented a first analysis of SN II spectra from CSP. The full analysis of that sample (optical and near IR photometry and spectroscopy) promises to significantly further our knowledge of the SN II phenomenon.

REFERENCES

Anderson, J. P., González-Gaitán, S., Hamuy, M., et al. 2014, ApJ, in press (arXiv:1403.7091)
Andrews, J. E., Gallagher, J. S., Clayton, G. C., et al. 2010, ApJ, 715, 541
Arcavi, I., Gal-Yam, A., Cenko, S. B., et al. 2012, ApJL, 756, L30
Barbon, R., Ciatti, F., & Rosino, L. 1979, A&A, 72, 287
Baron, E., Branch, D., Hauschildt, P. H., et al. 2000, ApJ, 545, 444
Branch, D., Falk, S. W., Uomoto, A. K., et al. 1981, ApJ, 244, 780
Cappellaro, E., Danziger, I. J., & Turatto, M. 1995, MNRAS, 277, 106
Chugai, N. N., Chevalier, R. A., & Utrobin, V. P. 2007, ApJ, 662, 1136
Folatelli, G., Morrell, N., Phillips, M. M., et al. 2013, ApJ, 773, 53
Hamuy, M. 2003, ApJ, 582, 905
Hamuy, M., Folatelli, G., Morrell, N. I., et al. 2006, PASP, 118, 2
Hamuy, M., & Pinto, P. A. 2002, ApJL, 566, L63
Inserra, C., Pastorello, A., Turatto, M., et al. 2013, A&A, 555, A142
Inserra, C., Turatto, M., Pastorello, A., et al. 2011, MNRAS, 417, 261
Inserra, C., Turatto, M., Pastorello, A., et al. 2012, MNRAS, 422, 1122
Kotak, R., Meikle, W. P. S., Farrah, D., et al. 2009, ApJ, 704, 306
Leonard, D. C., Filippenko, A. V., Ardila, D. R., & Brotherton, M. S. 2001, ApJ, 553, 861
Leonard, D. C., Filippenko, A. V., Gates, E. L., et al. 2002a, PASP, 114, 35
Leonard, D. C., Filippenko, A. V., Li, W., et al. 2002ba, AJ, 124, 2490
Litvinova, I. I., & Nadezhin, D. K. 1983, Ap&SS, 89, 89
Litvinova, I. Y., & Nadezhin, D. K. 1985, SvAL, 11, 145
Milisavljevic, D., Fesen, R. A., Kirshner, R. P., & Challis, P. 2009, ApJ, 692, 839
Pastorello, A., Ramina, M., Zampieri, L., et al. 2005, in Proc. of IAU Colloq., Vol. 192, Cosmic Explosions, On the 10th Anniversary of SN1993J, ed. J. M. Marcaide & K. W. Weiler (Berlin: Springer), 195
Pastorello, A., Sauer, D., Taubenberger, S., et al. 2006, MNRAS, 370, 1752
Pastorello, A., Zampieri, L., Turatto, M., et al. 2004, MNRAS, 347, 74
Patat, F., Barbon, R., Cappellaro, E., & Turatto, M. 1994, A&A, 282, 731
Pooley, D., Lewin, W. H. G., Fox, D. W., et al. 2002, ApJ, 572, 932
Popov, D. V. 1993, ApJ, 414, 712
Sahu, D. K., Anupama, G. C., Srividya, S., & Muneer, S. 2006, MNRAS, 372, 1315
Schlegel, E. M. 1996, AJ, 111, 1660